Free-standing graphene membranes on glass nanopores for ionic current measurements

Michael I. Walker,[1] Robert S. Weatherup,[2] Nicholas A. W. Bell,[1] Stephan Hofmann,[2] and Ulrich F. Keyser[1]

[1] *Cavendish Laboratory, University of Cambridge, J.J. Thomson Avenue, Cambridge CB3 0HE, United Kingdom*

[2] *Department of Engineering, University of Cambridge, Cambridge CB3 0FA, United Kingdom*

A method is established to reliably suspend graphene monolayers across glass nanopores as a simple, low cost platform to study ionic transport through graphene membranes. We systematically show that the graphene seals glass nanopore openings with areas ranging from 180nm^2 - 20μm^2, allowing detailed measurements of ionic current and transport through graphene. In combination with *in situ* Raman spectroscopy, we characterise the defects formed in ozone treated graphene, confirming an increase in ionic current flow with defect density. This highlights the potential of our method for studying single molecule sensing and filtration.

There is great potential for graphene monolayers in micro and nano fluidics [1]. Graphene's mechanical strength enables free standing atomically thin membranes [2] and theoretical approaches suggest these could, with appropriate pores, exhibit high performance, size selective filtration [3, 4]. Applications for graphene membranes include molecular sieving, water filtration and desalination [5, 6]. Progress has been made towards achieving this in studies of nanoporous sheets of graphene that have been shown to filter by size of molecule for both gases [7] and ionic solutions [8]. Porous graphene has been created by using ion/electron beam etching [9], exposure to UV light and ozone [10] or oxidative etching [11].

Free standing graphene membranes can be studied by placing the graphene on a porous substrate, where much of the graphene is supported [8]. Alternatively MEMS fabrication techniques are used to suspend isolated areas, up to ~50μm^2, of graphene but often involve many processing steps [10, 12, 13]. Here, we present a simple technique to expedite the study of free standing graphene membranes separating two liquid reservoirs by combining them with glass nanopores in a hybrid system. Glass nanopores formed by pulling hollow glass capillaries, heated at the center by a laser, so that they taper to a fine tip were developed for use in patch clamp experiments but have found uses in a wide range of fields [14]. They provide a robust and cheap platform for studying flexible membranes such as lipid bilayers [15] and DNA origami nanopores [16]. The diameter of the nanopore, which is determined by the pulling parameters, can range from tens of nanometers to a few microns.

In this paper we demonstrate a straightforward method to suspend graphene monolayers across glass nanopores as a rapid and reliable means to manipulate and study graphene membranes. The graphene seals the tip, significantly reducing the ionic current flow into the glass nanopore. We show that the measured ionic current flow is due to current flow through the membrane and demonstrate that we can detect the extent of defects in ozone damaged graphene. We quantify the effect of the ozone treatment by measurements of ionic transport and Raman spectroscopy.

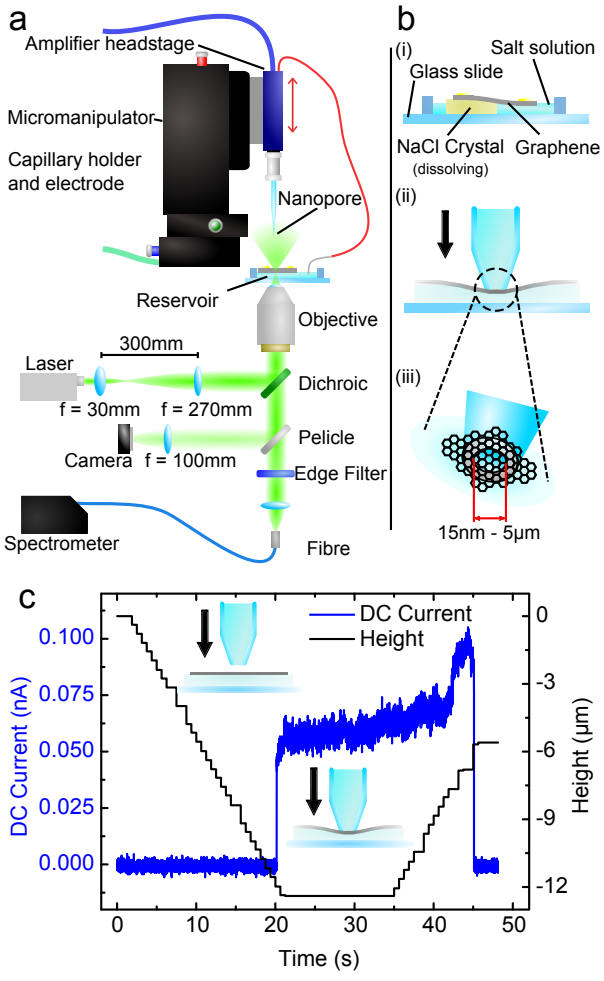

Figure 1. a) Diagram of the experimental setup showing the nanopore mounted on a micromanipulator and *in situ* Raman spectrometer. b) (i) Graphene is floated by dissolving a salt crystal into a reservoir. (ii) The graphene is then sealed onto the nanopore. (iii) This places a graphene monolayer across the tip of the glass nanopore. c) Current and nanopore height traces for a typical drive down and seal onto a graphene membrane floating on 1M NaCl, with a 400nm glass nanopore and 10mV bias. When the nanopore lands on the graphene membrane the current increases and the computer controlled drive down stops. The nanopore is then lifted up away from the surface until the current returns to the initial value.

Figure 1a shows the setup used to place graphene on the tip of a glass nanopore by pushing it vertically into a graphene monolayer floating on the surface of a reservoir (Figure 1b). The glass capillary, filled with an aqueous solution of 1M NaCl, is mounted on a micromanipulator *(Scientifica, Patch Star)* positioned above a custom made inverted microscope which images the water surface to acquire *in situ* Raman spectra. The reservoir is mounted on a purpose built x, y, z translation stage and Ag/AgCl electrodes in the capillary and reservoir are connected to an amplifier *(Axopatch 200B)*. LabVIEW software *(National Instruments, 2009)* is used to control the micromanipulator, apply voltages and record all measurements. The micromanipulator is used to position the nanopore above the graphene and lower it down whilst the current between the two electrodes is monitored. Contact between the glass nanopore and the graphene is detected when the current increases and the drive down of the nanopore is stopped. A typical drive down and retraction trace is shown in Figure 1c.

We form nanopores by pulling glass capillaries *(Sutter and Hilgenberg GmbH)* using a laser-based capillary puller *(Sutter P2000)* as described before [17]. In this work nanopores from five different pulling programs are used with diameters from 15nm to 5µm (further details in supplementary information).

Graphene is grown by chemical vapour deposition (CVD), in a custom built cold wall reactor, using 25µm thick platinum foil *(Alfa Aesar, 99.99%)* as the catalyst and C_2H_4 as the precursor [18–21] (details in supplementary information). The CVD grown graphene is polycrystalline with large grain sizes of 20-100µm, as confirmed by scanning electron microscopy of a sample for which growth was interrupted prior to complete coverage. It is transferred by spin coating a polymer *(polymethylmethacrylate, 4wt% in anisole, 950K molecular weight)* on to the surface and releasing the graphene from the catalyst by an electrolysis-based bubbling technique [19, 22, 23]. The polymer supported graphene is floated on an aqueous solution saturated with NaCl, allowing it to be lifted out onto the surface of a cleaved single crystal of NaCl *(SPI-Chem)*, without significant dissolution of the substrate. The sample is then dried at ∼50°C, and the polymer dissolved by immersion in acetone. Finally Au, with a thickness of 30nm, is thermally evaporated through a shadow mask to form thin stripes on the graphene to aid locating the membranes in our inverted microscope. The graphene is floated on the surface of the liquid by placing the salt crystal into the reservoir and allowing it to dissolve to yield a 1M NaCl solution. The reservoir is a microfluidic cell designed to limit evaporation, whilst ensuring a thin film of water (100-200µm) to facilitate imaging.

The inverted microscope is used to find, verify and characterise the graphene on the nanopore at the tip of the capillary by *in situ* Raman spectroscopy. The objective *(Olympus ACHN 40XP)* is used to focus a 532nm laser *(Laser Quantum Gem, CW, 532nm, 100mW)* onto the graphene. The reflected light is separated using a dichroic mirror *(Semrock 532nm RazorEdge)*, filtered using an edge filter *(Semrock 532nm EdgeBasic)* and the resulting spectra measured *(Ocean Optics, Ventanna 532nm)*. The microscope allows the graphene to be found on the surface of the reservoir, first by optically locating gold strips and then focusing the laser onto the adjacent graphene to record a Raman spectrum.

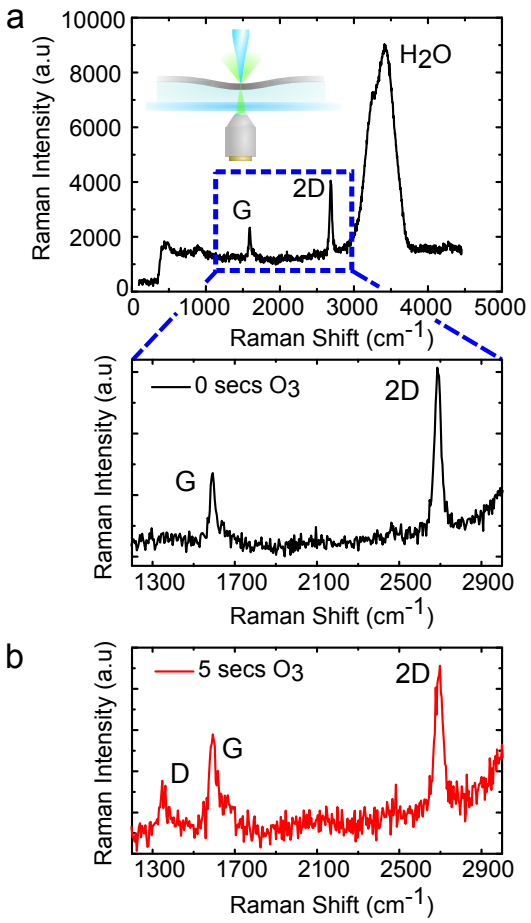

Figure 2. a) Raman Spectra obtained from as grown graphene floating on water showing a large peak due to the water and background from the glass slide. The magnified section of the spectrum shows the characteristic Raman spectrum of graphene. The ratio of the indicated G to 2D peaks indicates monolayer and the absence of a D peak indicates a low defect density. b) Typical Raman spectrum from ozone damaged graphene floating on water. The D peak is clearly visible after the sample was exposed to ozone for 5 seconds.

We can characterise the quality of graphene sheets floating on the water surface. A typical Raman spectrum for a graphene membrane floating on the surface of the reservoir is shown in Figure 2a. The two main graphene peaks are clearly visible at ∼1600cm^{-1} (G Peak) and ∼2690cm^{-1} (2D Peak) [24] and there is a signifi-

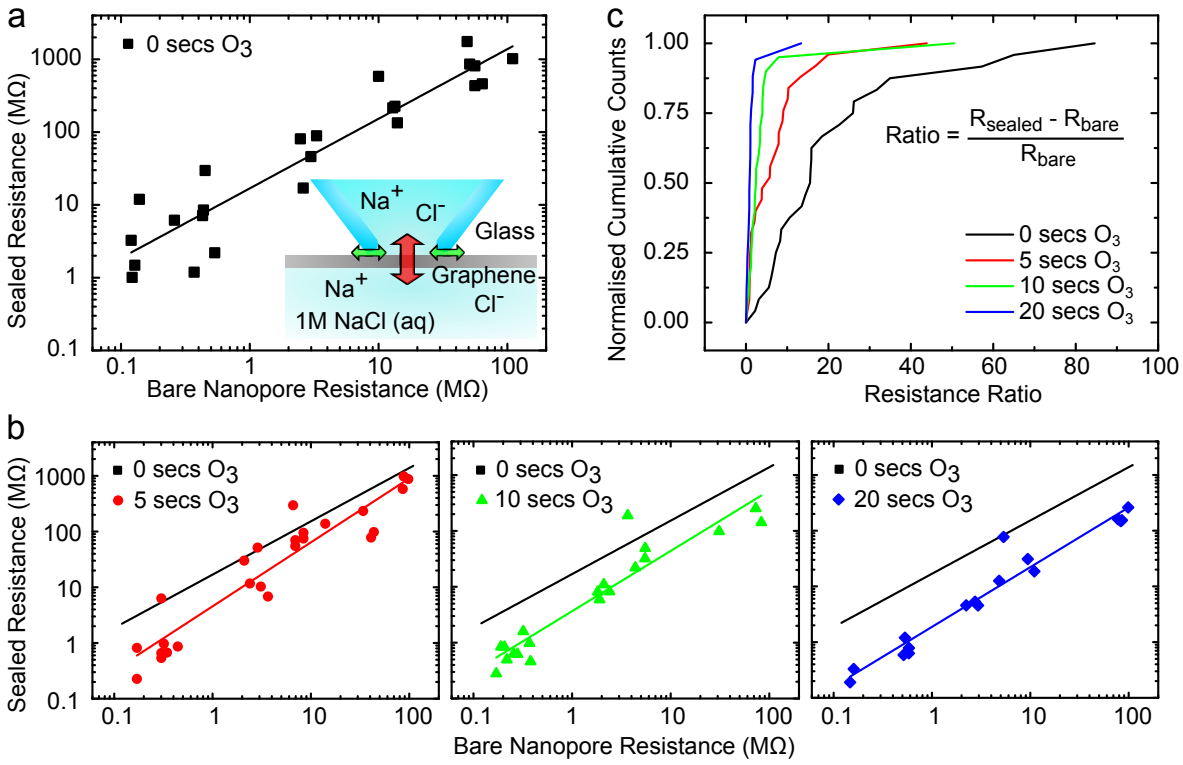

Figure 3. a) Resistance of nanopores sealed on as grown graphene plotted against the bare nanopore resistance. The gradient of the fitted line is 0.957 ± 0.075. This shows that the sealed resistance is directly proportional to the bare resistance and hence proportional to the area, indicating that the current measured is due to transport through the graphene. inset) Schematic of nanopore-graphene interface showing possible current routes; through the graphene membrane (red arrow) or around the perimeter (green arrows). b) Resistance of nanopores sealed on to graphene damaged by exposure to ozone. The fit to as grown samples is shown on each graph for comparison. For 5 secs O_3 exposure the gradient of the fit is 1.15 ± 0.087, for 10 secs O_3 the gradient is 1.08 ± 0.091 and for 20 secs O_3 the gradient is 1.07 ± 0.066. c) Plot of cumulative resistance ratio $(R_{sealed} - R_{bare})/R_{bare}$ normalised to number of experiments for each of the graphene samples. This ratio is independent of the area. The resistance of the graphene membranes decreases with ozone damage.

cant peak from the water corresponding to OH stretching modes (3000-4000cm^{-1}) [25]. We are not able to resolve any significant differences between the Raman spectra of graphene floating on water compared to graphene which has been transferred on to SiO_2.

To show that we can detect graphene properties such as defect density we investigated ozone damaged graphene. Graphene samples were damaged by exposing them to ozone for 5 - 20secs [26] (details in supplementary information). The damaged graphene is distinguished in Raman spectroscopy by the growth of the D peak ($\sim$1350cm^{-1}) indicating the presence of defects [27]. Figure 2b shows a typical Raman spectrum on water after 5 secs ozone treatment; further treatment causes the D peak to increase and subsequently the 2D to G peak ratio to decrease (data not shown) [28].

To apply our method to assess membrane quality we must first verify that the observed current is due to transport through the graphene. Inset Figure 3a shows a schematic illustration of the proposed ionic current flow through the graphene membrane and the alternative route around the perimeter of the nanopore. We evaluate the ionic current through the graphene membrane by recording an I-V curve and investigate the variation when using different sizes of glass nanopore. Before each experiment we determine the resistance of the bare nanopore in solution and then seal it on to a graphene membrane (example in supplementary information). A reduction in current, compared to the bare nanopore, indicates that the graphene has sealed across the tip of the nanopore. The sealed resistances range from 1-2GΩ for 15nm nanopores to 1-10MΩ for 5µm nanopores, although we note that these resistances are lower than other published values [12]. We observe a linear relationship between the sealed and bare resistances on as grown graphene (Figure 3a). As the resistance of the bare nanopore is inversely proportional to its area it follows that the sealed resistance scales with the area of the graphene on the tip. We can therefore conclude that the primary conduction route is through the graphene membrane. Given that a single crystal graphene membrane is expected to be impermeable [29, 30], we attribute the

current observed to intrinsic defects in the CVD grown graphene and assume there is no charge transfer to the graphene. The graphene domain sizes are larger than our glass nanopores, but it is likely that a proportion of the measurements with the larger diameters will capture grain boundaries contributing to the variation we observe in sealed resistances.

In order to demonstrate that our method can indeed detect ionic transport through damaged samples we analysed the ozone treated samples described above. Figure 3b shows that the resistance of the damaged graphene membranes decreases compared to the as grown sample, but the linear dependence with the bare nanopore resistance remains. The slightly non-linear relationship between sealed and bare resistances for graphene damaged with ozone for 5 secs is an indication that the induced defects are more widely spaced than the size of the smallest glass nanopore. This means that the smallest nanopores may seal onto an area of graphene which has not been affected by the ozone treatment. With increased ozone exposure time the number of defects is sufficiently high that all of the nanopores sample the defect distribution evenly, so the sealed resistances are inversely proportional to the area of graphene. The ratio between the sealed resistance and the bare resistance is a measure of the resistance of the graphene membrane independent of the area. Cumulative counts of this ratio for all of the experiments illustrate how the resistance of the graphene decreases with ozone treatment (Figure 3c). The effect of the ozone induced defects is visible in the both the Raman spectra and the electrical characterisation where we see that the defects provide additional routes for ionic transport.

We can assess the defect density of our graphene sheets by estimating the area through which ionic current is flowing. For this we calculated an effective total defect area directly from the resistance, assuming that the thickness of the graphene layer is 0.6 nm [12]. This gives an average defect area for a graphene membrane suspended across 180nm^2 (15nm diameter) pores of 0.11nm^2, equivalent to a single defect with a diameter of 0.38nm. Under the assumption that only one defect is captured by the 180nm^2 pore, we can use this defect size to calculate the defect density for our as grown and damaged graphene samples from the measurements using the larger nanopores. This assumption is supported by the non-linearity we observe and this defect size corresponds with typical values from literature [11]. We find that the average defect density in our as-grown graphene is $8 \times 10^9\text{cm}^{-2}$, increasing to $5 \times 10^{11}\text{cm}^{-2}$ in the sample which has been exposed to ozone for 20 secs. This assumes that ozone treatment induces new defects in preference to enlarging existing defects. These values are comparable to defect densities measured for CVD grown graphene [11] and consistent with the defect densities extracted from our measurements of the Raman D peak intensity [28].

We propose to use this platform to investigate the transport of different molecules through graphene monolayers incorporating defects and pores. Developing methods to control pore sizes and distribution will allow selective filters to be investigated. Another promising application for graphene membranes is nanopore sensing [31]. Nanopores in graphene membranes formed by TEM drilling [10, 12, 13] have been demonstrated for single molecule sensing and could result in high resolution for use in DNA sequencing [32]. Our technique will facilitate studies of pore formation and translocations of single molecules for nanopore sensing.

We have demonstrated a method for sealing graphene on the tips of glass nanopores with simultaneous, *in situ* characterisation by Raman spectroscopy. Varying the glass nanopore area has shown that our approach measures the ionic current flow through graphene membranes. Applying our technique to ozone damaged graphene has allowed us to study the effect of defects on ionic transport. Our method enables further studies of transport through graphene membranes for filtration and sensing applications.

The authors would like to thank S. Purushothaman and K. Göpfrich for careful reading of the manuscript and V. Thacker for useful discussions. This work was supported by the EPSRC Cambridge NanoDTC, EP/G037221/1 and EPSRC grant GRAPHTED, EP/K016636/1. RSW acknowledges a Research Fellowship from St. John's College, Cambridge. NAWB acknowledges an EPSRC doctoral prize award.

[1] A. K. Geim, Science **324**, 1530 (2009).
[2] C. Lee, X. Wei, J. W. Kysar, and J. Hone, Science **321**, 385 (2008).
[3] D. Jiang, V. R. Cooper, and S. Dai, Nano Letters **9**, 4019 (2009).
[4] K. Sint, B. Wang, and P. Král, J. Am. Chem. Soc. **130**, 16448 (2008).
[5] D. Cohen-Tanugi and J. C. Grossman, Nano Letters **12**, 3602 (2012).
[6] M. E. Suk and N. R. Aluru, The Journal of Physical Chemistry Letters **1**, 1590 (2010).
[7] S. P. Koenig, L. Wang, J. Pellegrino, and J. S. Bunch, Nature Nanotechnology **7**, 728 (2012).
[8] S. C. O'Hern, C. A. Stewart, M. S. H. Boutilier, J.-C. Idrobo, S. Bhaviripudi, S. K. Das, J. Kong, T. Laoui, M. Atieh, and R. Karnik, ACS Nano **6**, 10130 (2012).
[9] C. J. Russo and J. A. Golovchenko, Proceedings of the National Academy of Sciences of the United States of America **109**, 5953 (2012).
[10] C. A. Merchant, K. Healy, M. Wanunu, V. Ray, N. Peterman, J. Bartel, M. D. Fischbein, K. Venta, Z. Luo, A. T. C. Johnson, and M. Drndić, Nano Letters **10**, 2915 (2010).
[11] S. C. O'Hern, M. S. H. Boutilier, J.-C. Idrobo, Y. Song, J. Kong, T. Laoui, M. Atieh, and R. Karnik, Nano Let-

ters **14**, 1234 (2014).
[12] S. Garaj, W. Hubbard, A. Reina, J. Kong, D. Branton, and J. A. Golovchenko, Nature **467**, 190 (2010).
[13] G. F. Schneider, S. W. Kowalczyk, V. E. Calado, G. Pandraud, H. W. Zandbergen, L. M. K. Vandersypen, and C. Dekker, Nano Letters **10**, 3163 (2010).
[14] C. A. Morris, A. K. Friedman, and L. A. Baker, The Analyst **135**, 2190 (2010).
[15] S. Hernández-Ainsa, C. Muus, N. A. W. Bell, L. J. Steinbock, V. V. Thacker, and U. F. Keyser, The Analyst **138**, 104 (2013).
[16] N. A. W. Bell, V. V. Thacker, S. Hernández-Ainsa, M. E. Fuentes-Perez, F. Moreno-Herrero, T. Liedl, and U. F. Keyser, Lab on a Chip **13**, 1859 (2013).
[17] L. J. Steinbock, O. Otto, C. Chimerel, J. Gornall, and U. F. Keyser, Nano Letters **10**, 2493 (2010).
[18] R. S. Weatherup, B. C. Bayer, R. Blume, C. Ducati, C. Baehtz, R. Schlögl, and S. Hofmann, Nano Letters **11**, 4154 (2011).
[19] R. S. Weatherup, B. Dlubak, and S. Hofmann, ACS Nano **6**, 9996 (2012).
[20] P. R. Kidambi, C. Ducati, B. Dlubak, D. Gardiner, R. S. Weatherup, M.-B. Martin, P. Seneor, H. Coles, and S. Hofmann, The Journal of Physical Chemistry C **116**, 22492 (2012).
[21] R. S. Weatherup, H. Amara, R. Blume, B. Dlubak, B. C. Bayer, M. Diarra, M. Bahri, A. Cabrero-Vilatela, S. Caneva, P. R. Kidambi, M.-B. Martin, C. Deranlot, P. Seneor, R. Schloegl, F. Ducastelle, C. Bichara, and S. Hofmann, J. Am. Chem. Soc. **136**, 13698 (2014).
[22] Y. Wang, Y. Zheng, X. Xu, E. Dubuisson, Q. Bao, J. Lu, and K. P. Loh, ACS Nano **5**, 9927 (2011).
[23] R. S. Weatherup, C. Baehtz, B. Dlubak, B. C. Bayer, P. R. Kidambi, R. Blume, R. Schloegl, and S. Hofmann, Nano Letters **13**, 4624 (2013).
[24] A. C. Ferrari and D. M. Basko, Nature Nanotechnology **8**, 235 (2013).
[25] Y. Tominaga, A. Fujiwara, and Y. Amo, Fluid Phase Equilibria **144**, 323 (1998).
[26] M.-B. Martin, B. Dlubak, R. S. Weatherup, H. Yang, C. Deranlot, K. Bouzehouane, F. Petroff, A. Anane, S. Hofmann, J. Robertson, A. Fert, and P. Seneor, ACS Nano **8**, 7890 (2014).
[27] M. Lucchese, F. Stavale, E. M. Ferreira, C. Vilani, M. Moutinho, R. B. Capaz, C. Achete, and A. Jorio, Carbon **48**, 1592 (2010).
[28] L. G. Cançado, A. Jorio, E. H. M. Ferreira, F. Stavale, C. A. Achete, R. B. Capaz, M. V. O. Moutinho, A. Lombardo, T. S. Kulmala, and A. C. Ferrari, Nano Letters **11**, 3190 (2011).
[29] V. Berry, Carbon **62**, 1 (2013).
[30] J. S. Bunch, S. S. Verbridge, J. S. Alden, A. M. van der Zande, J. M. Parpia, H. G. Craighead, and P. L. McEuen, Nano Letters **8**, 2458 (2008).
[31] J. J. Kasianowicz, E. Brandin, D. Branton, and D. W. Deamer, Proc. Natl. Acad. Sci. USA **93**, 13770 (1996).
[32] D. B. Wells, M. Belkin, J. Comer, and A. Aksimentiev, Nano Letters **12**, 4117 (2012).